RSC Advances




ROYAL SOCIETY OF CHEMISTRY

www.rsc.org/advances

A table of contents entry for:

# Controllably Tuning the Near-infrared Plasmonic Modes of Gold Nanoplates for Enhanced Optical Coherence Imaging and Photothermal Therapy

Xueqin Jiang[a], Renming Liu[b], Peijun Tang[a], Wanbo Li[a], Huixiang Zhong[a], Zhangkai Zhou[b], and Jianhua Zhou[a]*

X. Q. Jiang, W. B. Li, H. X. Zhong, Prof. J. H. Zhou

[a] Biomedical Engineering Department, School of Engineering, Sun Yat-sen University, Guangzhou 510275, China

R. M. Liu, Dr. Z. K. Zhou

[b] State Key Laboratory of Optoelectronic Materials and Technologies, School of Physics and Engineering, Sun Yat-sen University, Guangzhou 510275, China

*Corresponding author:

Tel.: +86 20 39387890; Fax: +86 20 39387890

E-mail: zhoujh33@mail.sysu.edu.cn (J.H. Zhou).

Ozone can be used to precisely tailor the plasmon mode of gold triangular nanoprism for enhancing optical imaging and therapy.

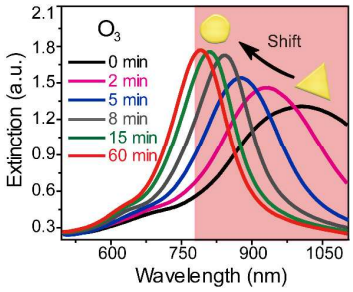

# Controllably Tuning of the Near-infrared Plasmonic Modes of Gold Nanoplates for Enhanced Optical Coherence Imaging and Photothermal Therapy

Xueqin Jiang[a], Renming Liu[b], Peijun Tang[a], Wanbo Li[a], Huixiang Zhong[a], Zhangkai Zhou[b], and Jianhua Zhou[a]*

X. Q. Jiang, W. B. Li, H. X. Zhong, Prof. J. H. Zhou

[a] Biomedical Engineering Department, School of Engineering, Sun Yat-sen University, Guangzhou 510275, China

R. M. Liu, Dr. Z. K. Zhou

[b] State Key Laboratory of Optoelectronic Materials and Technologies, School of Physics and Engineering, Sun Yat-sen University, Guangzhou 510275, China

*Corresponding author:

Tel.: +86 20 39387890; Fax: +86 20 39387890.

E-mail: zhoujh33@mail.sysu.edu.cn (J.H. Zhou)

## ABSTRACT

Tuning the localized surface plasmon modes of gold nanostructures into resonant with near-infrared incident light is desirable in various applications such as biosensing, biomedicine/therapy and opto-electronic devices. Unfortunately, current methods for regulating the plasmon modes of gold nanoparticles still suffered from poor controllability and reproducibility. Here, we developed a facile and effective method to precisely tailor the plasmon mode of gold triangular nanoprisms (GTNPs) by simply exposing them to $O_3$ atmosphere. The resonant wavelength of the plasmon mode sustained by the GTNPs can be steadily tuned over a broad spectral range varying from 1010 nm to 780 nm (within the bio-window region), along with their shapes gradually changing from triangular nanoprism into circular nanoplate. By controlling the concentrations of $O_3$, exposing duration, the concentrations of surfactant in suspension and the reaction temperature, GTNPs with various plasmon modes could be efficiently obtained from one original GTNPs sample. To demonstrate the potential applications of these GTNPs, we applied this method to obtain gold nanoplates as-needed for enhanced optical coherence tomography (OCT) and photothermal therapy. The plasmon mode of GTNPs was tuned to match the excitation wavelength of OCT laser source, and was applied to enhance the signal of OCT imaging. The plasmon mode of GTNPs was also precisely tuned to 808 nm which was well resonant with the wavelength of a near-infrared excitation laser ($\lambda_{ex}$ = 808 nm); when the as-obtained GTNPs were used as photothermal agent, they displayed an enhanced effect of photothermal therapy on Hela cancer cells compared

to those without the tuning of plasmon mode. Considering the simplicity and high controllability of the method for fine-tuning plasmonic mode of GTNPs, this work has great potential in a wide range of applications such as biomedical imaging and thermotherapy, chemical/biological sensing, surface-enhanced spectroscopy and solar energy harvesting etc.

**KEYWORDS:** *gold triangular nanoprism, near-infrared, localized surface plasmon resonances, plasmon mode tuning, optical coherence tomography, photothermal therapy*

## 1. INTRODUCTION

Local surface plasmon resonances (LSPRs) supported by gold nanostructures have received considerable attentions for their potential to facilitate extensive applications including biosensing[1-4], biomedical imaging[5-7] and phototherapy[8, 9], surface plasmon enhanced spectroscopy[10], catalysis[11], solar energy harvesting[12, 13] and so forth. Most of these applications are based on their attractive optical properties, especially the virtue of selective light-absorption at near-infrared wavelengths[14]. For instance, in the field of bioimaging or phototherapy, gold nanomaterials with plasmon resonance band locating in the near-infrared (NIR) range (700-1200 nm) are cultivated, so as to match the applied incident light with the wavelength in biological optical window, where optical absorption and scattering induced by tissues can be maximally reduced[15]. Also, the plasmon mode of gold nanostructure is usually regulated to agree with the long wavelength of the light source for optical devices[16]. Take solar cells as an example, the plasmon modes of gold nanostructures are engineered to match the solar spectrum at near-infrared region for the maximal utilizing of solar energy and enhancement of energy conversion efficiency[17]. Therefore, the capability for controllably tuning the plasmon mode of gold nanostructures at the wavelengths of near-infrared plays a pivotal role in constructing biomedical and opto-electronic applications, and further stimulates a wide range of interest in plasmonics[18, 19].

Therefore extensive research efforts have been devoted into the generation of gold nanostructures with near-infrared plasmonic modes, as well as the exploring of

plasmon mode controlling. To date, two general strategies are proposed. One strategy is to control the morphology of gold nanoparticles, and the other is to encapsulate the gold nanoparticles with other materials; because the plasmonic modes rely highly on their morphologies and the refractive indexes of the coating materials on the gold surface.[15, 20]. Correspondingly, chemical and physical synthesis routes are employed to control the morphologies of plasmonic nanostructure. However, the chemical approach usually exhibits poor controllability and reproducibility; For another, the physical methods such as photon lithography, electron-beam lithography, and ion beam lithography which suffer from problems of poor crystallization, low throughput and high cost, are also not favorable for practical application[21, 22].

On the other hand, manipulating the dielectric surrounding environment of metallic nanostructures was also reported as an alternative approach to realize the tuning of plasmon mode. Although many materials such as biological molecules[12, 23], polymers[5, 24, 25], inorganic materials[26, 27], are encapsulated around nanostructures for plasmon mode tailoring, these methods always manifest limited tuning range in spectral region. For example, by coating gold nanorods with silica, even the thickness of silica shell reaches up to 25.5 nm, the plasmon mode of the gold nanorods shifted only by ~50 nm, which was not sufficient to satisfy practical demands[28]. Therefore, it is necessary to develop simple and effective methods for tuning the plasmon mode of nanostructures with high controllability and large tuning spectral range in near-infrared region.

Here, we present a facile strategy for controllable tuning the plasmon mode of a

typical gold nanostructure, *i.e.* gold triangular nanoprisms (GTNPs). We choose GTNPs as an example because of its excellent optical properties. Compared to spherical gold nanoparticles, gold nanorods, and gold nanocages, GTNPs with anisotropic structures exhibit plasmon mode in a broader range from visible to infrared spectral region (covering the biological optical window of tissue), and show higher electric field enhancement for LSPR sensing, surface enhanced Raman, surface enhanced fluorescence and photoenergy conversion owing to their sharp corners[29-31]. In this work, we manage to precisely control the plasmon mode of GTNPs within the bio-window region by simply exposing the GTNPs suspension to $O_3$ gas. When the GTNPs are exposed to $O_3$, their sharp corners are gradually rounded and their plasmon mode experiences a significant blue-shift up to ~200 nm. The GTNPs with on-demand plasmon mode can be effectively achieved by controlling the reaction rate and the termination of the blue-shifting process. As examples of application, we applied this method to tune the plasmon modes of gold nanoplates into resonance with the emission of NIR lasers, leading to a significant increment of signal intensity in optical coherence tomography (OCT) imaging as well as an improved performance in photothermal damage on Hela cancer cells. Our findings not only introduce a facile, effective way to obtain the GTNPs with as-needed plasmon modes for biomedical applications, but also demonstrate GTNPs as a potential component for optical devices.

## 2. RESULTS AND DISCUSSION

### 2.1 Changes in Plasmonic Modes and Morphologies of Gold Nanoplates

Highly purified GTNPs were synthesized by using a mature seed-mediated protocol[30, 31], which involved the reduction of $HAuCl_4$ by L-ascorbic acid in the presence of gold seeds, potassium iodide (KI) and cetyltrimethylammonium bromide (CTAB), followed by a surface area-based purification process as we previously reported[32]. The synthetic process is detailed in the Experimental Section. As shown in Figure 1, the as-prepared GTNPs have two plasmon modes observed in the extinction spectrum (the black line). The one appearing at about 652 nm comes from the weak quadrupole plasmon resonance, while the other locating at 1004 nm is originated from the strong dipole plasmon mode[33]. Then, after exposing the GTNPs suspension to $O_3$ (75 ppm) prepared by a household ozone generator or to atmosphere which always contains $O_3$ (~0.01 to 0.12 ppm), the extinction spectra gradually blue-shift with duration time (as shown in Figure 1 and S1A). To specific, in the total exposure time of 60 min, the resonant wavelength of the dipole plasmon mode at 1004 nm experiences significant changes in the NIR spectral region (as shown in the red region of Figure 1), undergoing a blue shift by 214 nm (from 1004 to 790 nm). This sensitive response of the GTNPs to $O_3$ in principle promises an approach for tuning the plasmon mode of GTNPs. In addition, the absorption intensity of the GTNPs increases by 0.461 (from 1.306 to 1.767) which is 35% of the preliminary absorption intensity. The enhancement in the absorption intensity may improve photothermal performance and benefit to corresponding applications. Furthermore, despite the dramatic changes in the dipole plasmon mode, the quadrupole plasmon mode at 652

nm only has a slight change by ~40 nm during the same exposing process, indicating that the plate-like morphology of the GTNPs were well preserved when exposed to $O_3$. There is no need to prolong the exposure time because we found the GTNPs suspension exhibited no further spectral variation after 1 h.

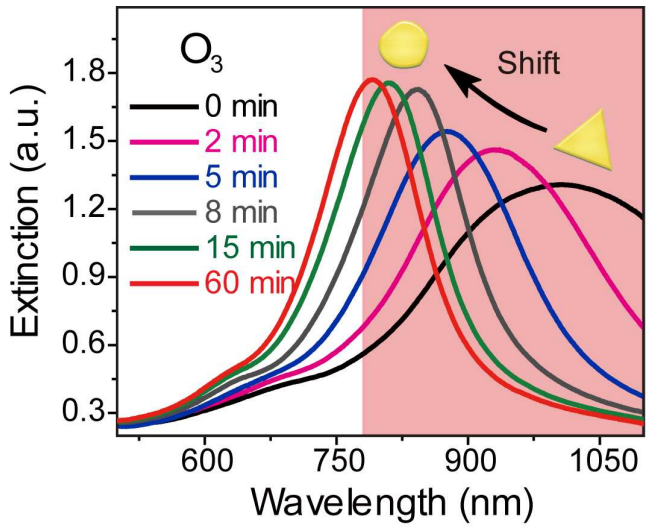


**Figure 1.**Time-dependent UV-vis extinction spectra of GTNPs when exposed to $O_3$ (75 ppm) for different periods of time. The dipole plasmon mode of GTNPs blue-shifts from 1004 nm to 790 nm in the NIR region (as shown as the red region). The insets show the shape transformation of the GTNPs with the shift of their plasmon mode.

In contrast to the significant shift of the plasmon mode when the GTNPs suspension was exposed to $O_3$, no obvious change of the plasmon mode was found when the GTNPs suspension was placed in a closed bottle (the suspension was isolated from an atmosphere which always contains $O_3$), and the plasmon modes of the GTNPs in the closed bottle are very stable for a few months' preservation (Figure S1B). This suggested that, unlike the spontaneous shift of the plasmon mode sustained

by silver nanoprism[29] that is sensitive to atmosphere, the shift of the dipole plasmon mode from GTNPs are really caused by the exposure to $O_3$. To further verify this conclusion, exposing experiments of the GTNPs to different gases (*e.g.* $O_2$, CO, $SO_2$, $N_2$, $CO_2$), which widely exist in atmosphere, were also conducted, but no shifts of the plasmon mode appeared in these experiments (as shown in Figure S2), illustrating that such a typical shift of wavelength was not from other gases in atmosphere but $O_3$.

Also, the shifting rate of the plasmon mode was found related to the concentrations of $O_3$. When the concentration of $O_3$ was as high as 75 ppm, the plasmon mode shifted rapidly by ~13 nm per min, making it difficult to precisely control the shifting process and to obtain the GTNPs with on-demand plasmon mode. However, the shifting rate slowed down obviously when the GTNPs were exposed to $O_3$ with lower concentrations (as shown in Figure S3). In order to control of the shifting process of the plasmon mode, we chose to conduct the exposing experiments in $O_3$ with relatively low concentrations (~0.04 to ~0.12 ppm) in the following demonstrations. These results confirmed that $O_3$ is the key factor for the tuning of plasmon mode. The reaction between $O_3$ and the GTNPs is that the gold atoms at the sharp corners of the GTNPs were preferentially oxidized and dissolved, because these corners are high-energy sites. Oxidative etching may play a significant role in rounding the corners of the GTNPs. The etching of a nanostructure usually starts from the sites with sharp features, such the corners of the GTNPs; because the GTNPs are rich in low-coordination atoms, and the dissolution of these atoms at the corners can reduce the total surface energy of the nanocrystal.[34-36].

Figure 2 shows the morphologies of the GTNPs before and after exposed to $O_3$ for different periods of time. Figure 2A displays a typical transmission electron microscope (TEM) image of the as-prepared GTNPs with three sharp corners and an average side length of 141±12 nm. Figure 2B-D present the GTNPs after exposed to $O_3$ (~ 0.08 ppm) for different durations of 2.5, 4 and 9 h, respectively. It is clearly seen that a manifestation of the morphological changes occurred to the GTNPs, which is consistent with the observed blue-shift of the dipole plasmon mode. Specifically, the sharp corners of the GTNPs are gradually rounded during the exposing process, eventually leading to the formation of gold circular nanoplates. Compared to the original triangular nanoprisms, the circular nanoplates have an obvious reduction in the lateral dimensions by 40 nm (with an average side length of 101 ± 9 nm), as well as an increase in the homogeneity which both contributed to the decrease of the full width at half maximum (FWHM) in the extinction spectra of Figure 1. It is also observed that the plate-like morphology was well preserved during the exposing process (also see the scanning electron microscope images in Figure S4), which is consistent with previous observation of the little shift of the quadrupole plasmon mode at 650 nm. These results stem from the different energies of the gold atoms on different facets. It has been investigated that the surface energies ($\gamma$) of gold crystallographic planes are not equivalent and generally scale accordingly: $\gamma\{111\} < \gamma\{100\} < \gamma\{110\}$[37], indicating that gold atoms on {111}facet (flat domain) are inerter than other surface atoms on {100} and {110} facets (side domain), thereby explaining the well preserved plate-like morphology of the GTNPs.

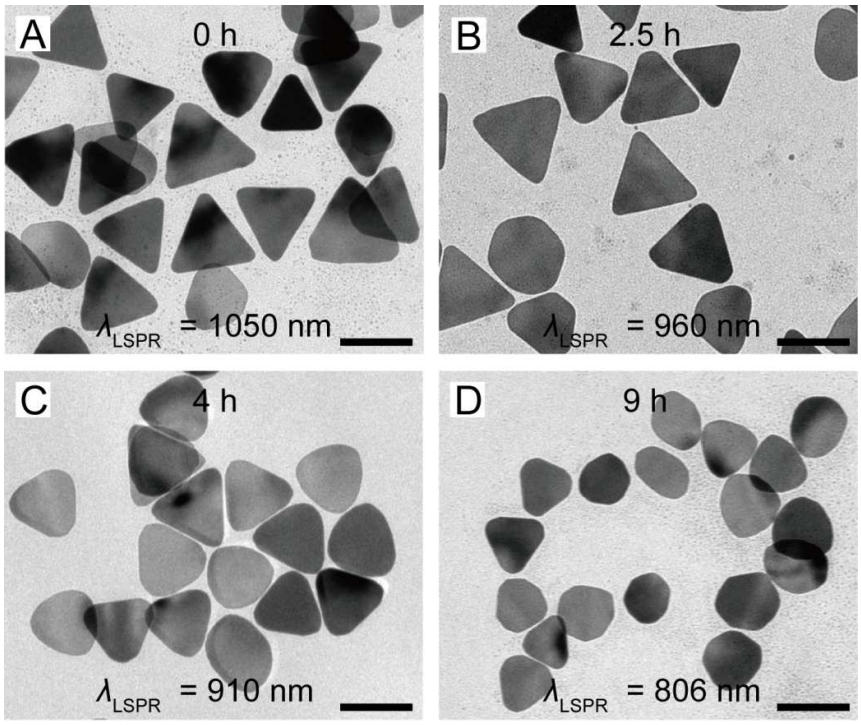


**Figure 2.** Morphologic changes of the GTNPs during the exposing process. Transmission electron microscope (TEM) images taken from the GTNPs exposed to $O_3$ (~ 0.08 ppm) for (A) 0 h, (B) 2.5 h, (C) 4 h, and (D) 9 h with their plasmon modes shifted to shorter wavelengths. The sharp corners of GTNPs were gradually rounded to form circular nanoplates. The scale bars represented 100 nm.

### 2.2 Controllably Tuning the Plasmonic Modes of Gold Nanoplates

For further understanding of the shift process of the plasmon mode supported by GTNPs, the temperature and the concentration of surfactant (CTAB) effects on spectral shift were also investigated. A series of GTNPs suspensions with different concentrations of CTAB (0, 0.15, 0.30, and 0.50 mM) were subjected to an exposing process in $O_3$ (~ 0.08 ppm) at room temperature. As shown in Figure 3A, in the case

without CTAB in suspension, the plasmon mode of the GTNPs experiences a rapid and distinct blue-shift in 210 min. However, while the concentration of CTAB in suspension was increased to 0.30 mM, the shift of the plasmon mode obviously slowed down (Figure 3B). The same phenomena can also be seen from Figure 3C, which summarizes the spectral shifts with various CTAB concentrations as a function of time, revealing that the shift rate of the plasmon mode decreases with the increase in the concentration of CTAB. This behavior results from the gradually formation of a close-packed CTAB bilayer on the surface of the GTNPs, which passivates the surface gold atoms[38], and thereby reduces the rate of the oxidative dissolution of the gold atoms at the sharp corners caused by the oxidation-reduction reaction between $O_3$ and the GTNPs. Moreover, the temperature was also found to have an influence on the shift process of the plasmon mode. Three different temperatures (*i. e.* 0 $^{o}$C, 23 $^{o}$C and 37 $^{o}$C) were carried out in $O_3$ ( ~0.08 ppm) without CTAB in suspensions. Figure 3D shows the peak location of the plasmon modes for three GTNPs suspensions as a function of time. It is clearly found that the shift rate of the plasmon modes has an evident relationship with temperature; the rates increase with the temperature rising. Although the concentration of the ozone dissolved in the suspension decreases at 37 $^{o}$C, the increase of temperature shows a more significant effect on accelerating the shape transformation of GTNPs. More normalized extinction spectra of the GTNPs (during the shift process) with the various concentrations of CTAB and different temperatures are displayed in Figure S5 and S6, respectively. Such different rates of spectral shift related to the concentration of CTAB and reaction temperature should be

useful for a precise control of the plasmon mode shifting process and thus help us to effectively acquire GTNPs with desired resonant wavelength.

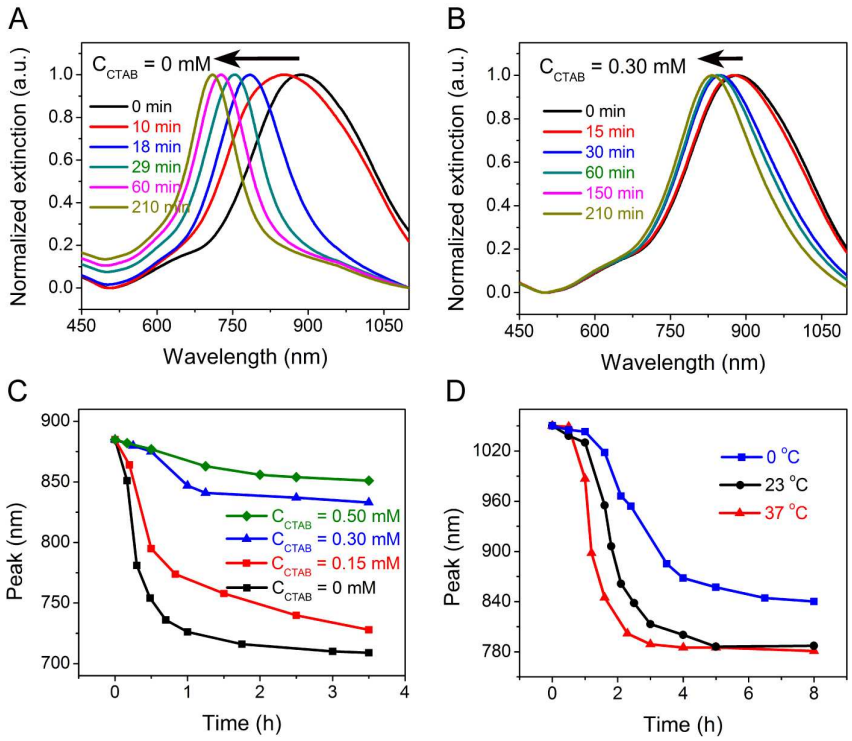


**Figure 3.** The rates of the plasmon mode shifts of GTNPs as a function of time at different conditions. Time-dependent normalized UV-vis extinction spectra taken from GTNPs suspensions exposed to $O_3$ in atmosphere (~ 0.08 ppm) at (A) 0 mM; (B) 0.30 mM CTAB in the suspension; and (C) Plasmon mode shifts of the GTNPs when exposed to $O_3$ (~ 0.08 ppm) at different concentrations of CTAB (0, 0.15, 0.30, 0.50 mM) in suspensions. (D) Plasmon mode shifts of the GTNPs when exposed to $O_3$ (~ 0.08 ppm) at different temperatures (0, 23 and 37 $^{o}$C) without CTAB in the suspension.

To fully demonstrate the potential of the exposing-to-$O_3$ approach as a facile and controllable method to obtain GTNPs with on-demand plasmon mode, we further

investigated the "stop" control of the shifting process for the plasmon mode. During the experiment, when the plasmon modes of the GTNPs reached the required plasmon mode, the suspension was immediately transferred to a sealed bottle, preventing it from $O_3$ in atmosphere. Actually, the shift of the plasmon mode did not stop immediately, due to the dissolved $O_3$ in the aqueous suspension (See Figure S7). So, in our experiments, preventing further spectral shift of GTNPs in sealed bottle became a pivotal issue. Fortunately, as we found in Figure 3C, adding CTAB into the suspensions can effectively terminate the shift process. Thus, we can suspend the shift of plasmon mode by adding CTAB into the suspensions. Also, for the purpose of a precise control, we select to use a low concentration of $O_3$ (~ 0.04 ppm) to regulate the plasmon mode of GTNPs. As a result, we are able to make the GTNPs experience a slow shift of the plasmon mode with a rate of 0.8 nm per min (Figure 4A), and obtain GTNPs with on-demand plasmon resonant wavelength by immediately transferring them from $O_3$ atmosphere to a sealed bottle with CTAB solution. The GTNPs protected by CTAB were found well maintained at a plasmonic mode with a little diverges of about $\pm 8$ nm in the following hours (Figure 4A), and this high stability of GTNPs will facilitate their future applications. Figure 4B gives the extinction spectra of the stable GTNPs we have achieved at each time point, where GTNRs with plasmon resonance wavelengths from 845 to 966 nm are presented. Based on the above demonstrations, we can regulate the shifting process of the plasmon mode of GTNPs by exposing it to ozone, then stopping the shifting process by the addition of CTAB, thereby achieve controllably and precisely tuning of the

plasmon modes within the bio-window region.

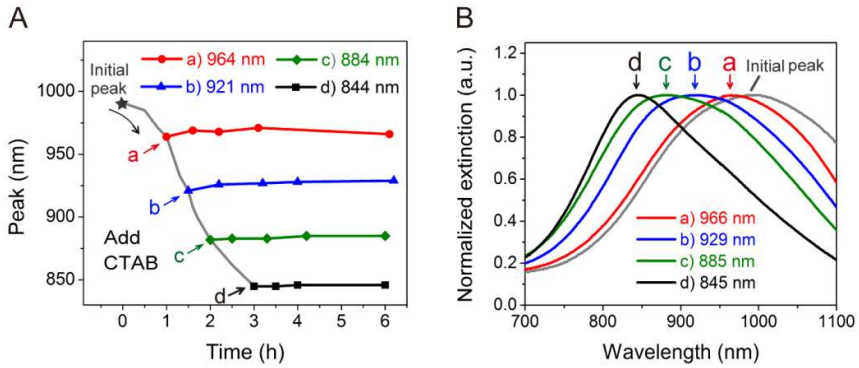


**Figure 4.** The controlled "shift" and "stop" of the plasmon mode of GTNPs regulated by the time period exposing to $O_3$ and adding of CTAB. (A) Plasmon mode shifts of the GTNPs suspension when exposed to $O_3$ (~ 0.04 ppm). When reaching the plasmon mode on-demand (at the points of a, b, c and d), CTAB solution (0.05 M) was added into the GTNPs suspension immediately to stop the shift of the plasmon mode. (B) Normalized UV-vis extinction spectra of the corresponding suspensions at the time points of a, b, c and d in (A).

### 2.3 Tuning the Overlapping between the Plasmon Modes of GTNPs and NIR Laser for Enhanced OCT imaging

After the realization of precisely controlling plasmon mode of the GTNPs, we turn to demonstrate the potential applications of the GTNPs with as-needed plasmonic modes for biomedical imaging and therapy. Here, we present an example on using GTNPs as a type of contrast agent for OCT imaging. OCT imaging is a non-invasive, three-dimensional medical imaging technique which has proved to be an efficient tool for imaging the segments of eye and skin with a spatial resolution of 5-15 μm[39].

OCT is based on low-coherence interferometry, typically employing NIR light for deeper penetration into the scattering medium for imaging. The GTNPs appear to be an excellent candidate for enhancing the OCT signal, because GTNPs with plasmon resonances in the NIR region can provide strong backscattering upon laser radiation, and their plasmon modes also can be controllably tuned to match the operating wavelength of the OCT laser source to achieve signal amplification [40].

We prepared GTNPs with plasmon modes at 1097, 926, and 860 nm (shown in Figure 5A) from one suspension of GTNPs by the above-mentioned approach. Their OCT images were then taken in agarose phantoms by an 840-nm OCT system with its emission spectrum presented in Figure 5A (the red line). Figure 5B shows the OCT image of the agarose phantom without GNTPs. The OCT image of agarose is poorly contrasted due to the low intensity of the scattered light. On the other hand, in the case of agarose phantom containing GTNPs with plasmon mode at 1097 nm, as shown in Figure 5C, the signal intensity is slightly improved, but it still shows weak enhancement of the images. However, for the GTNPs after the tuning process ($\lambda_{LSPR}$ = 926 and 860 nm), the intensities of their OCT images become stronger. (Figure 5D-E). The estimated signal intensity of GNTPs ($\lambda_{LSPR}$ = 860 nm) is 2.7 times greater than that of agarose, and 1.8 times greater than that of GNTPs ($\lambda_{LSPR}$ = 1097 nm) (Figure S8). The observable contrast enhancement of GTNPs for OCT images stems from the overlap between the plasmas of GTNPs and the laser source. When the plasmon mode is closed to the emission band of the OCT laser, it can yield a strong interaction between GTNPs and the excitation light, allow getting maximum enhancement of

backscattered light and provide a significant increment in signal intensity of OCT images[40]. Since gold nanoparticles has been successfully demonstrated as contrast agents for OCT imaging[6, 41], tuning the plasmon mode of GTNPs into resonance with OCT laser emission band can be considered a simple approach to improve the efficiency of gold nanoparticles in contrasting enhancement. Also, as the plasmon mode of gold nanoplates can be tuned broadly in NIR region, this method of regulating the plasmon mode of GTNPs to achieve better performance of gold nanoparticles may be adaptable in other optical devices for biomedical applications which usually operate light within the NIR region.

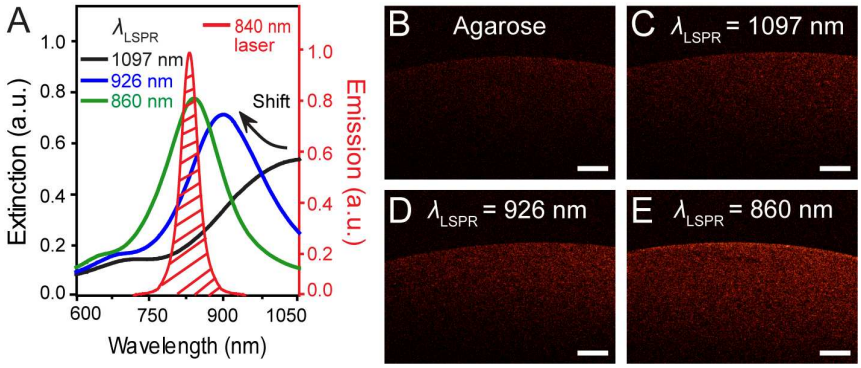


**Figure 5.** Tuning the plasmon mode of GTNPs to overlap with the wavelength of OCT laser for enhanced imaging. (A) Extinction spectra of the GTNPs suspension before (the black solid line) and after (the blue and green solid lines) the tuning process and the emission spectrum of the OCT laser with a central wavelength at 840 nm are shown (the red solid line); (B-E) OCT images of (B) Agarose, and the GTNPs-agarose phantoms containing GTNPs with surface plasmon modes at (C) 1097 nm, (D) 926 nm and (E) 860 nm. Scale bars are 300 μm.

### 2.4 Enhanced Photothermal Conversion Efficiency of Gold Nanoplates for Thermotherapy

We further demonstrate that the GTNPs with on-demand plasmon mode can act as a candidate of photothermal agents with enhanced photothermal conversion efficiency. The potential use of the GTNPs for thermotherapy is dependent on the penetration of light source into the tissue, as well as the ability of GTNPs to capture energy from the light source[42]. So, tuning the plasmon mode into resonant with the excitation source can improve the photothermal performance of the GTNPs. In this demonstration, we employed a NIR laser with a wavelength centered at 808 nm as excitation light source (shown as the red line in Figure 6A), this wavelength is favorable for biological applications as the extinction of light by water and fat in tissues at this wavelength is relatively low[14] (shown by the green dashed lines in Figure 6A). The GTNPs resonant with and isolated from the excitation wavelength are respectively prepared, and their extinction spectra are plotted as the pink and black curves in Figure 6A. A hydrogel channel composed of agarose and fat was applied as a simulated tissue in these experiments (Figure 6B). The photothermal experiments were carried out with the help of an IR camera. Figure 6C gives the infrared images of the channel loaded with the GTNPs ($\lambda_{LSPR}$ = 976 nm), and the temperature at the center of the channel increases from 24 $^{o}$C to 30 $^{o}$C after a laser irradiation of 4 min. However, when the channel was loaded with the GTNPs whose plasmon mode was tuned to 808 nm for well matching with the center wavelength of the NIR laser, the temperature at the center of the channel experienced a faster increase by 19 $^{o}$C, from

24 °C up to 43 °C (Figure 6D). The temperature of 43 °C enables an irreversible damage to the cancer cells or tissues due to the denaturation of biomolecules[43], which makes this GTNPs capable for thermotherapy. Such a notable improved capability of the GTNPs ($\lambda_{LSPR}$ = 808 nm) in elevating temperature is attributed to the tuning of the plasmon mode, as well as the increase in the absorption intensity of the GTNPs during the plasmon mode tuning process. The comparisons of photothermal experiment with GTNPs of $\lambda_{LSPR}$ = 976 and $\lambda_{LSPR}$ = 808 can be found in Figure S9. To sum, by precisely tuning the plasmon mode to match the laser wavelength, the photothermal conversion efficiency of the GTNPs can be significantly improved, which will hold promising potential for photothermal therapy.

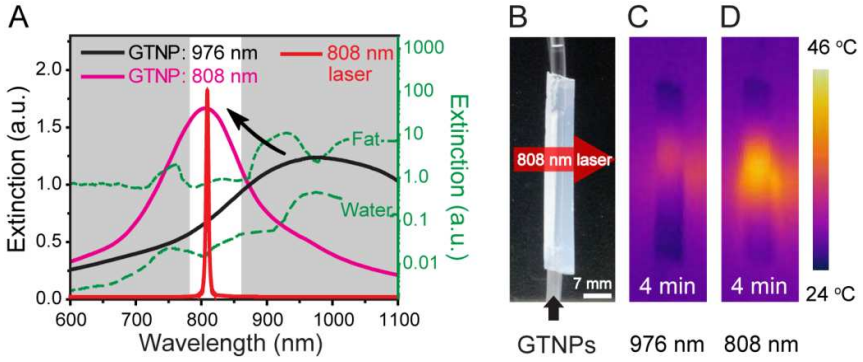


**Figure 6.** Precisely tuning the plasmon mode of GTNPs to the bio-window of tissue for the demonstration of photothermal conversion. (A) Extinction spectra of the GTNPs suspension before (the black solid line) and after (the pink solid line) the tuning process and the emission spectrum of an NIR laser used in these experiments with a central wavelength at 808 nm are presented (the red solid line). Extinction spectra of fat and water (the green dash lines) in this region as well as their relatively low extinction region (the white area) are also shown; (B) Photo of the agarose-fat channel as a simulated tissue. (C-D) The infrared images of the

channel loaded with the GTNPs suspensions with plasmon modes at (C) 976 nm and (D) 808 nm and then irradiated by the 808 nm NIR laser for 4 min. The temperatures at the center of the chip were up to 30 and 43 $^{o}$C for (C) and (D), respectively.

Following the demonstration of the photothermal conversion efficiency of the GTNPs, we utilize the GTNPs with $\lambda_{LSPR}$ = 808 nm as photothermal agent to destruct cancer cells *in vitro*. A type of Hela cancer cells which can stably express green fluorescence protein in alive were used in this experiment. Cell viability was monitored by using green fluorescence images of cancer cells before and after irradiation. Figure 7A shows the green fluorescence image of the Hela cancer cells in a mixture of agarose and GTNPs with $\lambda_{LSPR}$ = 808 nm before they are treated with laser irradiation. The green image indicates that the cancer cells are alive. After 1 min of NIR irradiation under a laser beam of 2 mm in diameter which is highlighted by the dashed circle (Figure 7B), this region basically has no green fluorescence, suggesting the loss of live cells. Furthermore, the diameter of the circular region well matches the laser spot size of 2 mm in diameter, confirming that the death of Hela cancer cell is caused by the photothermal destruction. Figure 7C demonstrates the green fluorescence image of the Hela cancer cells in the mixture of agarose and GTNPs ($\lambda_{LSPR}$ = 808 nm) after NIR irradiation for 4 min. It is clearly seen that the region of cells damaged increases with the irradiation duration and exceeds the irradiation beam spot size. This is expected because the heat harvested from NIR irradiation would increase with time and transferred to regions outside the irradiation beam spot. As a

comparison, the green fluorescence image of the control group (living Hela cancer cells in the agarose-GTNPs ($\lambda_{LSPR}$ = 969 nm) mixture after the treatment of NIR irradiation for 4 min) is shown in Figure 7D. One can see that, almost no essential changes in cell viability before and after the irradiation. These results indicate that the GTNPs with plasmon mode matching well with the excitation source possess a more effective performance in photothermal destruction of Hela cancer cells *in vitro*. So, our method for precisely tuning the plasmon mode to on-demand wavelength gives a rise to enhancement in the performance of GTNPs for photothermal therapy.

Although these results suggested that GTNPs show good promise for enhancing optical imaging and photothermal therapy, surface modification of GTNPs for higher biocompatibility and tumor-targeting capacity, the distribution and pharmacokinetics of GTNPs in vivo need to be investigated in the future studies.

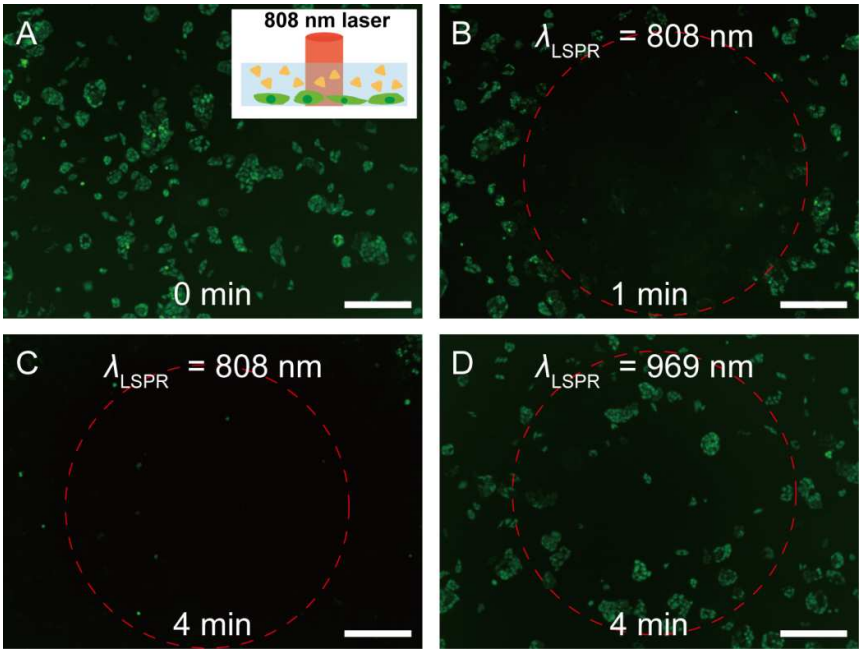


**Figure 7.** The photothermal effect of the GTNPs on cancer cells. Hela cancer cells (which stably expressed green fluorescent protein) were covered by a layer of hydrogel and GTNPs

($\lambda_{LSPR}$ = 808 nm) mixture, and then irradiated by an 808 nm laser beam at a power density of 2.0 W/cm$^2$ for different periods of time: (A) 0, (B) 1, (C) 4 min. The red dashed circles show the laser irradiation region. The green fluorescence images clearly show the size of the damaged area which lacks green fluorescence increases with the irradiation time. In contrast, (D) Hela cells covered by the hydrogel and GTNPs ($\lambda_{LSPR}$= 969 nm), and then irradiated under the same conditions for 4 min. The inset is the schematic illustration of the irradiation experiment.

## 3. CONCLUSION

In conclusion, we have developed a facile method to precisely regulate the plasmon modes of the GTNPs in a broad spectral range varying from 1004 to 790 nm. Our strategy is based on the preferentially oxidative dissolution of the gold atoms with high energy at the sharp corners by using $O_3$ gas, making the shape of gold nanoprism changing from triangular to circular. By controlling the experimental parameters of the GTNPs exposing to $O_3$ process, including the concentrations of $O_3$, exposing duration, the concentration of CTAB in suspensions and the reaction temperature, GTNPs with on-demand plasmon modes within the bio-window region can be easily obtained from one GTNPs sample. Compared with the published methods for tuning the plasmon mode of gold nanostructures, this exposing-to-$O_3$ method is facile, controllable, low cost and high efficient. The $O_3$ can come from atmosphere or an inexpensive household ozone generator. Also, as the GTNPs are easily spoiled by $O_3$ which is widely spread in atmosphere, the findings in this work will contribute to the

preparation and preservation of the GTNPs under laboratory conditions. We also demonstrated the applications of GTNPs with required plasmon mode as contrast agents for OCT imaging and as photothermal agents for photothermal therapy. The GTNPs with plasmon mode that well matched with the laser wavelengths showed advanced performances in enhancing OCT imaging and improving the efficiency of photothermal conversion for thermal damage on Hela cancer cells. We believe that this simple strategy for controllably tuning the plasmon mode of gold nanostructures would be interesting to a wide spectrum of researchers working in the field of nanophotonics, biosensing, biomedical imaging, and medical treatment, etc.

## 4. EXPERIMENTAL SECTION

**Materials.** Gold (III) chloride trihydrate ($HAuCl_4 \cdot 3H_2O$, >99.0%), sodium borohydride ($NaBH_4$, 99%), L-ascorbic acid ($C_6H_8O_6$, > 99%), potassium iodide (KI, 99%), were purchased from Aladin and used as received; cetyltrimethylammonium bromide (CTAB, 99%), trisodium citrate ($C_6H_5O_7Na_3 \cdot 2H_2O$, 99.00%), sodium hydrate (NaOH, 97.00%), sodium chloride (NaCl, 99.50%) were purchased from Tianjin Damao Chemical Reagent Factory; $O_3$ gas was produced by an ozone generator (M Fresh High-Tech Co,. Ltd, SW-250); the concentration of $O_3$ was recorded by an ozone detector (Beijing Qihongruida Co,. Ltd, MIC-800); Agarose with their gelling temperatures at 45 and 37 $^oC$ were purchased from Sigma and Biowest, respectively. In all experiments, we used deionized water with a resistivity of 18.2 MΩ·cm, which was prepared by a Millipore Mili-Q water system.

**The Synthesis and Purification of Gold Triangular Nanoprisms (GTNPs).** GTNPs with the dipole plamson resonance located within the NIR region were prepared following a seed-mediated method in aqueous solutions[30, 31]. All glasswares were washed with aqua regia (3:1 ratio by volume of HCl and $HNO_3$; CAUTION: Aqua Regia is highly toxic and corrosive), and rinsed copiously. Deionized water was employed throughout the experiments. Specifically, the seed suspension was made by adding a freshly prepared, ice-cold $NaBH_4$ solution (0.1 M, 1 mL) into a mixture solution made of $HAuCl_4$ (0.01 M, 1 mL) and trisodium citrate (0.01 M, 1 mL) as well as water (36 mL). The resultant solution was mixed by rapid inversion for 2 min and then kept at room temperature for 4 h before use for the hydrolysis of the surplus unreacted $NaBH_4$. Then three growth solutions (A, B, and C) were prepared for the seed-mediated growth. Solution A and B were identical, contained CTAB (0.05 M, 9.0 mL), KI (0.1 M, 4.5 μL), NaOH (0.1 M, 0.05 mL), ascorbic acid (0.1 M, 0.05 mL) and $HAuCl_4$ (10 mM, 0.25 mL). Solution C was made by mixing CTAB (0.05 M, 45 mL), KI (0.1 M, 0.023 mL), NaOH (0.1 M, 0.25 mL), ascorbic acid (0.1 M, 0.25 mL), and $HAuCl_4$ (10 mM, 1.25 mL). Note that all these solutions were prepared by adding agents in the sequence listed above. The formation of GTNPs was initiated by adding 1 mL of as-prepared seed solution into solution A, follow by gently shaken. Then 5 mL of growth solution A was quickly added to solution B and shacked slightly. 2.5 mL of solution B was added in to solution C. The reaction mixture was subjected to gentle inversion for 15 s and then left undisturbed for at least 1 h.

The 45 mL mixture contained expected GTNPs and byproduct gold spherical

nanoparticles. The separation were conducted by following a procedure modified previously reported method[32]. NaCl solution (4.0 M, 2 mL) was added into the resulting mixture, and the last mixed solution was left undisturbed for overnight. Then, the supernatant suspension was gently transferred from the glass beaker, while the GTNPs with a color of green remained sticking at the bottom. 20 mL water was added in to disperse the sediments. Finally, the GTNPs purified suspension with a plasmon mode at ~1010 nm was obtained.

**The Process of Exposing GTNPs to $O_3$.** 20 mL of the as-prepared GTNPs suspension was placed in a glass jar, kept it open and then placed in $O_3$ (~ 0.08 ppm) at room temperature (25 $^{o}$C) for different periods of time. During the exposing process, aliquots of the suspension were taken out subsequently from the jar at specific time for photographs, UV-vis extinction spectral recordings and TEM sample preparations.

The exposing experiments with various concentrations of CTAB in suspensions were conducted by following the similar above-mentioned procedures, but additionally adding various CTAB solutions into the each GTNPs suspension before the exposing process. Noted that the concentration of CTAB in the GTNPs suspension with no extra CTAB added in was considered to be 0 mM in this experiment. 15, 30, 50 μL of CTAB solutions (0.05 M) were added in different suspensions, respectively, to obtain the suspensions with 0.15, 0.30, 0.50 mM CTAB (5 mL for each), and then followed by the typical exposing process.

Another GTNPs suspension was divided into three glass jars for the time-temperature exposing experiments. The three aliquots of suspension were

exposed to $O_3$ (~ 0.08 ppm) in water baths at 0, 23 and 37 ℃, respectively. Also, samples were taken out at specific times for UV-vis extinction spectral recordings.

**Controlling the Terminations of the Plasmon Mode Shifting.** As soon as the plasmon mode of GTNPs suspension in the exposing process was observed reaching at the as-needed wavelength, the suspension was immediately transferred into a sealed bottle, followed by a quick addition of CTAB solution (0.05 M, 3 mL). After being shaken for 10 s, the suspension was incubated at room temperature for further use.

**Tuning the Plasmon Mode for the Investigation of the Enhanced OCT.** We performed OCT imaging in agarose phantoms to demonstrate the enhancement capability of gold nanoplates. Gold nanoplates with plasmon modes at 1097, 926, and 860 nm were prepared from a suspension of GTNPs based on the above-mentioned tuning method. The GTNPs-agarose phantoms were prepared in the following way: 0.3 g of agarose was added to 10 mL of water at boiling point under stirring. Afterwards, 1 mL of gold nanoplates suspensions were added into 1 mL of as-prepared agarose solution, following by stirring and cooling for the formation of GTNPs-agarose gel. All the three GTNPs-agarose tissue phantoms ($\lambda_{LSPR}$ = 1097, 926, and 860 nm) were analyzed with a optical coherence tomography imaging system (TEK SQRAY, HSO-2000) at a central wavelength of 840 nm (with a spectral bandwidth of 45 nm).

**Tuning the Plasmon Mode for the Investigation of the Efficiency of Temperature Increase.** An agarose-fat channel composed of water, agarose (gel point at 45 $^{o}$C) and fat was applied in these experiments. Specifically, 0.15 g of agarose was added in 10

mL deionized water and was boiled for 2 min. Then 0.3 g of fat was ultrasonically dispersed in the agarose solution. The mixture was quickly poured into a petri dish, buried a plastic pipe (d = 2 mm) and sat quietly for 30 min. The plastic pipe was then carefully pulled out. Thus the agarose-fat channel was ready.

GTNPs with plasmon mode at 976 nm were synthesized and were employed to the exposing process with the $O_3$ (~0.08 ppm), in order to tune the plasmon mode to exactly 808 nm, which is the plasmon mode optimally matched the NIR laser as well as the transparency of bio-tissue. The NIR irradiation was conducted with the power density of 2.0 W/cm$^2$ and the irradiation distance to the center of the channel fixed to 2.5 cm. First, the agarose-fat channel was loaded with the GTNPs ($\lambda_{LSPR}$ = 976 nm) and irradiated by the NIR laser for 4 min. The temperature increase was monitored by a NIR camera at specific time intervals. As the GTNPs ($\lambda_{LSPR}$ = 976 nm) was loaded-off, the channel was clean by pumped in deionized water for 3 min. The GTNPs ($\lambda_{LSPR}$ = 808 nm) was then loaded on, followed by similar NIR irradiation experiments as mentioned above.

**Demonstration of the GTNPs as photothermal agent for thermotherapy *in vitro*.** Fluorescent Hela cells were grown in Dulbecco's modified Eagle's medium/High Glucose (DMEM/High Glucose) supplemented with 1% antibiotics and 10 % new born bovine serum (NBS). The cultures were incubated at 37 ℃ in a humidified atmosphere containing 5% $CO_2$ and the medium was changed every other day. Fluorescent Hela cells were then seeded in two 24-well plates for 1 day and rinsed three times with PBS for further experiments. A GTNPs-agarose mixture were

prepared by mixing GTNPs suspension (75 μL) with a 0.3 % (w/w) agarose solution (50 $^{o}$C, 75 μL) whose gel point was 37 $^{o}$C. After intensively stirring, the GTNPs became well-dispersed with a stable plasmon mode (Figure S10). The GTNPs-agarose mixture was slightly added into the cell wells and covered the Hela cells with a thickness of 1.5 mm, followed by adding 150 μL of medium. The Hela cells were then irradiated with a NIR laser with a center wavelength at 808 nm and a power density of 2.0 W/cm$^2$ with the irradiation spot size on the GTNPs-agarose mixture fixed to 2 mm. The green fluorescence images were captured before and after irradiations for evaluation of the cell viability. The green fluorescence imaging of the Hela cells were captured by a fluorescent inverted microscope (Olympus, TH4-20G).

**Characterization of Samples.** TEM images were captured by using a microscope (FEI Tecnai G2 Spirit) operated at 120 kV. The samples for TEM studies were prepared by drying a drop of the aqueous suspension of the GTNPs on a piece of carbon-coated copper grid (Zhongjing Technology Corporation). The samples were dried and stored in a vacuum for TEM characterization. The UV-vis extinction spectra were obtained using a UV-vis spectrophotometer (Inesa L3S). The temperature increase of the agarose-fat channel was monitored by an IR camera (FLIR E30). The concentration of $O_3$ was measured by an ozone detector (Beijing Hongqiruida Corporation, MIC-800).

## ASSOCIATED CONTENT

### Supporting Information

Electronic Supplementary Information (ESI) available: Normalized UV-vis absorption spectra taken from solution exposed to air and time-depended normalized UV-vis extinction spectra of GTNPs suspension which was sealed in a bottle for several months; the influence of different types of gases in air on the plasmon mode shifts of GTNPs; the effect of ozone with different concentrations on the plasmon mode shifts of GTNPs; scanning electron microscope (SEM) images of the GTNPs during the exposing process; the rates of the plasmon mode shifts of GTNPs with different concentrations of CTAB in the suspension; the rates of the plasmon mode shifts of GTNPs at different temperatures; the stop of the plasmon mode shifting with and without adding CTAB; enhancement of OCT signal using GTNPs with different plasmon modes; the temperature of the center of the channel loaded on with GTNPs obtained plasmon modes of 808 nm and 976 nm under radiation of a 808 nm laser; a schematics showing the wavelength of the NIR laser and UV-vis extinction spectra of GTNPs-agarose mixtures used in the demonstrations of thermotherapy.

## AUTHOR INFORMATION

**Corresponding Author**

*E-mail: zhoujh33@mail.sysu.edu.cn.

**Notes**

The authors declare no competing financial interest.

## ACKNOWLEDGMENTS

We thank Prof. Hongkai Wu for the nice discussion. This work was supported in part by the National Natural Science Foundation of China (21405183), the project for Science & Technology New Star of Zhujiang in Guangzhou City (2013J2200048) and Guangdong Innovative Research Team Program（No. 2009010057).

REFERENCES

1 C. K. Wu, C. Xiong, L. J. Wang, C. C. Lan and L. S. Ling, *Analyst*, 2010, **135**, 2682-2687.
2 H. J. Wu, J. Henzie, W. C. Lin, C. Rhodes, Z. Li, E. Sartorel, J. Thorner, P. D. Yang and J. T. Groves, *Nat. Methods*, 2012, **9**, 1189-1191.
3 W. B. Li, X. Q. Jiang, J. C. Xue, Z. K. Zhou and J. H. Zhou, *Biosens. Bioelectron.*, 2015, **68**, 468-474.
4 W. B. Li, L. Zhang, J. H. Zhou and H. K. Wu, *J. Mater. Chem. C*, 2015, 6479-6492.
5 M. Chen, S. H. Tang, Z. D. Guo, X. Y. Wang, S. G. Mo, X. Q. Huang, G. Liu and N. F. Zheng, *Adv. Mater.*, 2014, **26**, 8210-8216.
6 B. Wang, L. Kagemann, J. S. Schuman, H. Ishikawa, R. A. Bilonick, Y. Ling, I. A. Sigal, Z. Nadler, A. Francis, M. G. Sandrian and G. Wollstein, *PloS one*, 2014, **9**, e90690.
7 T. T. Chi, Y. C. Tu, M. J. Li, C. K. Chu, Y. W. Chang, C. K. Yu, Y. W. Kiang and C. C. Yang, *Opt. Express*, 2014, **22**, 11754-11769.
8 M. Perez-Hernandez, P. del Pino, S. G. Mitchell, M. Moros, G. Stepien, B. Pelaz, W. J. Parak, E. M. Galvez, J. Pardo and J. M. de la Fuente, *ACS Nano*, 2014, **9**, 52-61.
9 D. Kim, Y. Y. Jeong and S. Jon, *ACS Nano*, 2010, **4**, 3689-3696.
10 Y. Wang, M. Becker, L. Wang, J. Q. Liu, R. Scholz, J. Peng, U. Goesele, S. Christiansen, D. H. Kim and M. Steinhart, *Nano Lett.*, 2009, **9**, 2384-2389.
11 K. Nishioka, S. Horita, K. Ohdaira and H. Matsumura, *Sol. Energy Mater. Sol. Cells*, 2008, **92**, 919-922.
12 J. Nam, S. Park and C. A. Mirkin, *J. Am. Chem. Soc.*, 2002, **124**, 3820-3821.
13 G. Tagliabue, H. Eghlidi and D. Poulikakos, *Nanoscale*, 2013, **5**, 9957-9962.
14 Y. N. Xia, W. Y. Li, C. M. Cobley, J. Y. Chen, X. H. Xia, Q. Zhang, M. X. Yang, E. C. Cho and P. K. Brown, *Acc. Chem. Res.*, 2011, **44**, 914-924.
15 N. Li, P. X. Zhao and D. Astruc, *Angew. Chem., Int. Ed.*, 2014, **53**, 1756-1789.
16 O. L. Muskens, V. Giannini, J. A. Sanchez-Gil and J. G. Rivas, *Nano Lett.*, 2007, **7**, 2871-2875.
17 J. R. Cole and N. J. Halas, *Appl. Phys. Lett.*, 2006, **89**, 153120.
18 Y. B. Zheng, L. L. Jensen, W. Yan, T. R. Walker, B. K. Juluri, L. Jensen and T.

J. Huang, *J. Phys. Chem. C*, 2009, **113**, 7019-7024.
19 L. J. E. Anderson, C. M. Payne, Y. R. Zhen, P. Nordlander and J. H. Hafner, *Nano Lett.*, 2011, **11**, 5034-5037.
20 W. L. Barnes, A. Dereux and T. W. Ebbesen, *Nature*, 2003, **424**, 824-830.
21 S. J. Hurst, E. K. Payne, L. Qin and C. A. Mirkin, *Angew. Chem., Int. Ed.*, 2006, **45**, 2672-2692.
22 Z. K. Zhou, D. Y. Lei, J. M. Liu, X. Liu, J. C. Xue, Q. Z. Zhu, H. J. Chen, T. R. Liu, Y. Y. Li, H. B. Zhang and X. H. Wang, *Adv. Opt. Mater.*, 2014, **2**, 56-64.
23 V. Mani, B. V. Chikkaveeraiah, V. Patel, J. S. Gutkind and J. F. Rusling, *ACS Nano*, 2009, **3**, 585-594.
24 Y. Leroux, J. C. Lacroix, C. Fave, G. Trippe, N. Felidj, J. Aubard, A. Hohenau and J. R. Krenn, *ACS Nano*, 2008, **2**, 728-732.
25 N. Jiang, L. Shao and J. F. Wang, *Adv. Mater.*, 2014, **26**, 3282-3289.
26 W. L. Gao, G. Shi, Z. H. Jin, J. Shu, Q. Zhang, R. Vajtai, P. M. Ajayan, J. Kono and Q. F. Xu, *Nano Lett.*, 2013, **13**, 3698-3702.
27 B. Tangeysh, K. M. Tibbetts, J. H. Odhner, B. B. Wayland and R. J. Levis, *Nano Lett.*, 2015, **15**, 3377-3382.
28 Q. Q. Zhan, J. Qian, X. Li and S. L. He, *Nanotechnol.*, 2010, **21**, 055704.
29 J. Zeng, S. Roberts and Y. N. Xia, *Chem. Eur. J.*, 2010, **16**, 12559-12563.
30 J. E. Millstone, S. J. Hurst, G. S. Metraux, J. I. Cutler and C. A. Mirkin, *Small*, 2009, **5**, 646-664.
31 J. E. Millstone, W. Wei, M. R. Jones, H. Yoo and C. A. Mirkin, *Nano Lett.*, 2008, **8**, 2526-2529.
32 R. M. Liu, J. H. Zhou, Z. K. Zhou, X. Q. Jiang, J. M. Liu, G. H. Liu and X. H. Wang, *Nanoscale*, 2014, **6**, 13145-13153.
33 Z. X. Li, Y. Yu, Z. Y. Chen, T. R. Liu, Z. K. Zhou, J. B. Han, J. T. Li, C. J. Jin and X. H. Wang, *J. Phys. Chem. C* 2013, **117**, 20127-20132.
34 Y. Q. Zheng, J. Zeng, A. Ruditskiy, M. C. Liu and Y. N. Xia, *Chem. Mater.*, 2014, **26**, 22-33.
35 Y. J. Xiong, *Chem. Commun.*, 2010, **47**, 1580-1582.
36 M. N. O'Brien, M. R. Jones, K. L. Kohlstedt, G. C. Schatz and C. A. Mirkin, *Nano Lett.*, 2014, **15**, 1012-1017.
37 J. S. DuChene, W. X. Niu, J. M. Abendroth, Q. Sun, W. B. Zhao, F. W. Huo and W. D. Wei, *Chem. Mater.*, 2012, **25**, 1392-1399.
38 B. Nikoobakht and M. A. El-Sayed, *Langmuir*, 2001, **17**, 6368-6374.
39 E. V. Zagaynova, M. V. Shirmanova, M. Y. Kirillin, B. N. Khlebtsov, A. G. Orlova, I. V. Balalaeva, M. A. Sirotkina, M. L. Bugrova, P. D. Agrba and V. A. Kamensky, *Phys. Med. Biol.*, 2008, **53**, 4995-5009.
40 Y. Ponce de León, J. L. Pichardo-Molina, N. Alcalá Ochoa and D. Luna-Moreno, *J. Nanomater.*, 2012, **2012**, 1-9.
41 M. Kirillin, M. Shirmanova, M. Sirotkina, M. Bugrova, B. Khlebtsov and E. Zagaynova, *J. Biomed. Opt.*, 2009, **14**, 021017.
42 J. Y. Chen, C. Glaus, R. Laforest, Q. Zhang, M. X. Yang, M. Gidding, M. J. Welch and Y. N. Xia, *Small*, 2010, **6**, 811-817.

43 K. H. Song, C. Kim, C. M. Cobley, Y. Xia and L. V. Wang, *Nano Lett.*, 2009, **9**, 183-188.